Numerical study of the *3D*-shape of a drop immersed in a fluid under an elongational flow with vorticity

Numerical study of the *3D*-shape of a drop immersed in a fluid under an elongational flow with vorticity

A S Sanjuan[1], M A H Reyes [2], A A Minzoni[3] and E Geffroy[1]
[1]Instituto de Investigaciones en Materiales, Universidad Nacional Autónoma de México, Mexico City.
[2]Departamento de Termofluidos, Facultad de Ingeniería. Universidad Nacional Autónoma de México, Mexico City.
[3]Instituto de Investigaciones en Matemáticas Aplicadas y en Sistemas., Universidad Nacional Autónoma de México, Mexico City.

E-mail: alfrsj07@gmail.com

Abstract. This work focuses on a three-dimensional analysis of the deformation of a drop —immersed in a Newtonian fluid— generated by a 2D elongational flow with vorticity. The study of steady-state deformations of the cross-section of the drop shows a prevalent non-circular shape. The axisymmetric idealization of the ellipsoid is not observed nor the linear dependency between capillary number and deformation of the drop, as Taylor and Cox theory predicted. Our numerical results are consistent with experiments and other numerical simulations. However, in the latter cases, measurements of the cross section of the drop are few while a limited class of flows is applied. In this work, deformations induced by general two-dimensional flows upon the 3D drop shape are presented with special emphasis about the length scale along the third axis —perpendicular to the plane of the applied flow field.

1. Introduction

Flow-induced drop deformation is an important topic in Fluid Mechanics [1,2] due to applications in industry as emulsion processing, micro-fluidics technologies [3-5], and others. Since the work of Taylor [1,2] the study of drop deformation has focused in the effects induced by the flow applied on the continuum phase. As Rallison explains [3], studies of drop deformations have focused principally when it is subjected to shear flows or extensional flows. The analysis of these two-dimensional flows permitted the theoretical analysis of small-drop deformation [1,3,5,6], assuming an spheroidal shape with the cross-section remaining axisymmetric. However, Guido et all [7] found that cross-sections in simple shear flow are non circular. Numerical studies of drop deformation showed this conditions [5,8], but these studies did not analyze the drop cross-section.

The study of drop deformation in two-dimensional flows is still an open question because an ample family of 2D-flows is not easily carried out in the laboratory [9-11]. As we will see in the next Section, a family of 2D-flows ranging from simple shear to pure extensional flow can be obtained as a mixture of rotation and elongation parts [1,12]. With this family of flows, it is possible to study the drop deformations induced from simple shear to extensional flow, while observing the contribution of added vorticity in the flow. The numerical experiments here presented can supplement the experimental data to understand better the dynamics of drop deformations.

This work focuses in flows with kinematics close to those of simple shear flow but, with less vorticity —more elongational effects. To calibrate the numerical experiments, the experimental data of Rosas et al., [10] are used.

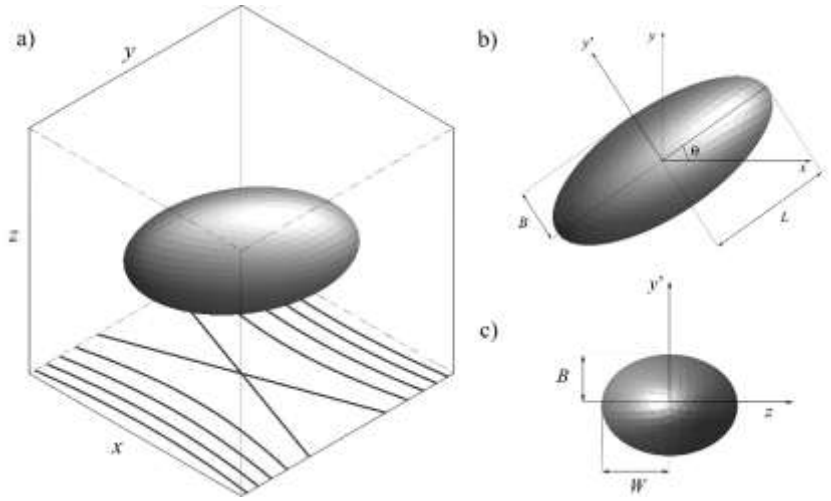

Figure 1. Scheme of a two-phase fluid. Drop in stationary shape. $\lambda_\mu = 0.012$, $\alpha = 0.13$, $Ca = 0.4$.
a) 3D-view view of the drop within a 2D-flow applied.
b) Conventional perspective on the *xy* plane.
c) Cross section of the drop.

2. Drop deformation in 2-D linear flow

The analysis of drop deformation assumes two Newtonian fluids, figure 1. The first (inner) phase is the drop with viscosity μ_0 and surface tension σ. The continuum phase has a viscosity μ_1. The viscosity ratio is $\lambda_\mu = \mu_0/\mu_1$. The two fluids have the same density and both are immiscible. There is not surfactant and there are not Marangoni stresses present. The creeping-flow conditions are assumed. In the creeping-flow regime the fluid motion is governed by the Stokes equations [12]

$$\mu\nabla^2\boldsymbol{u} = \nabla p\,,$$
$$\nabla\cdot\boldsymbol{u} = 0\,. \tag{1}$$

The velocity $\boldsymbol{u}$ is continuous at the drop interface *S*. The tractions exerted on the two sides of the interface between the two fluids have two different values, with a corresponding discontinuity:

$$\Delta\boldsymbol{f} = \boldsymbol{f}_1 - \boldsymbol{f}_0 = (\Pi_1 - \Pi_0)\cdot\hat{\boldsymbol{n}}\,, \tag{2}$$

where $\hat{\boldsymbol{n}}$ is the normal vector pointing out of *S*. In this work, a constant value surface tension [13] is assumed; i.e., $\nabla\cdot\hat{\boldsymbol{n}}$ is equal to twice the mean curvature κ_m at that point on the interface,

$$\Delta\boldsymbol{f} = \sigma\hat{\boldsymbol{n}}\nabla\cdot\hat{\boldsymbol{n}} = 2\sigma\kappa_m\hat{\boldsymbol{n}} \tag{3}$$

The drop is subject to a two dimensional linear incident flow

$$\boldsymbol{u}(x,y) = \frac{G}{(1+\alpha)}(\alpha\, y, x)\,, \tag{4}$$

where G is the intensity of the rate of deformation tensor [15] and the flow parameter is α [9-11, 14].

$$G = \left(\left|\boldsymbol{II}_{2D}\right|\right)^{1/2}. \tag{5}$$

Equation (4) assumes that the α parameter goes from zero to one. The case $\alpha = 0$ corresponds to simple shear flow with the velocity gradient in the *y* direction, the value of G is equal to shear rate $\dot{\gamma}$. For $\alpha = 1$ we have an extensional flow in two-dimension with the principal axes of deformation at $x = y$ —the compressional axes being $x = -y$; the intensity of the flow is the strain rate $\dot{\varepsilon}$.

The dynamic of drop deformation is characterized by three dimensionless numbers. The viscosity ratio λ_μ, the capillary number *Ca* equation (6) and The flow parameter α equation (7). The capillary number characterizes the ratio between viscous stresses —imposed by the flow— and capillary forces that resist the deformation and drive the drop towards the equilibrium shape, were r_0 is the non-deformed radius of the drop.

$$Ca = \frac{r_0\mu_1 G}{\sigma}\,, \tag{6}$$

Finally, the flow parameter α characterizes the magnitude of the rotational component relative to the extensional component of the external flow. Here, results are presented for a range of values of the flow-parameter close to simple shear flow, i.e., $\alpha = 0.03$, $\alpha = 0.05$ and $\alpha = 0.13$. The applied flow

covers a range of the Capillary number from *0.05* to *0.40*. For values less than the minimum, the drop shape does not present different values of its principal conditions; for values of *0.4* or less, the deformation is not significant to cause drop breakup. The continuum phase is more viscous than the drop viscosity: $\lambda_\mu = 0.012$; the value is chosen so that numerical predictions match the values of the experiment results of Rosas [10].

The measure of drop deformation used corresponds to Taylor Deformation:

$$D_T = \frac{L - B}{L + B}, \tag{7}$$

were *L* and *B* are the axes of the drop shown in figure 1. Additionally, we present the time evolution of the lengths of all principal axes of the drop *vs*. the initial radius; see figure 2.

3. Numerical Method

The numerical method used is the 3D collocation boundary element method [13]. Using the Lorentz reciprocal theorem for Stokes regime [12,13], particular solutions can be expressed in terms of known solutions as point sources on the interface where $\boldsymbol{u}_0$ is the flow on the surface of the drop and $\boldsymbol{f}_0$ is the force on the surface of the drop.

$$\int_S (\mu_1 \boldsymbol{u}_1 \boldsymbol{f}_0 - \mu_0 \boldsymbol{u}_0 \boldsymbol{f}_1) dS = 0, \tag{8}$$

were $\boldsymbol{f} = \boldsymbol{\sigma} \cdot \hat{\boldsymbol{n}}$, considering on the surface of the drop point sources whose velocity and stresses are the stokeslet and the stresslet respectively [5,12,13]. Then, the numerical scheme is represented as

$$\boldsymbol{u}^\infty(x_0) - \frac{1}{8\pi\mu_1}\int_S \Delta \boldsymbol{f}(x)\cdot \boldsymbol{G}(x,x_0)\, dS(x) + \frac{1-\lambda_\mu}{8\pi}\int_S \boldsymbol{u}_1(x_0)\cdot \boldsymbol{T}(x,x_0)\cdot \hat{\boldsymbol{n}}(x)\, dS(x) = \begin{cases} \boldsymbol{u}_1(x_0) & \text{a)}, \\ \dfrac{1+\lambda_\mu}{8\pi}\boldsymbol{u}_1(x_0) & \text{b), or} \\ \lambda_\mu \boldsymbol{u}_2(x_0) & \text{c)}. \end{cases} \tag{9}$$

In this equation there are three cases. The case, (b) Solves the velocity field when x_0 is on the surface of the drop. Then with this information the case (a) calculates the velocity field when x_0 is outside of the drop —exterior flow. Finally, (c) calculates the velocity field when x_0 is inside the drop.

The flow imposed on the continuum phase is determined by $\boldsymbol{u}^\infty(x_0)$. The second term on the left side of equation (9) is known as the Single Layer Potential and evaluates stresses across the interface. The third term is known as the Double Layer Potential and is used to evaluate the velocity field at the interface. The boundary element method has the advantage that it reduces the 3D computation problem into a 2D-evaluation, i.e., the method requires to solve the velocity field on the surface of the drop, and (b) with this information is possible to have the velocity field outside or inside the drop.

3.1 Numerical implementation of the computation of stresses and velocity fields

The numerical scheme solves the Stokes flow equation at an instant of time, equation (9 b). The evolution of the drop shape is carried out using the velocities obtained at the collocation points. By means of an interpolation subroutine the velocity at all nodes is calculated and then the new position of the drop is evaluated. For the evaluation of the Single Layer Potential, an approximation of the local curvature of the drop is used, using equation 3 with curved triangles. A quadratic interpolation throughout these triangles is performed to obtain the mean curvature of the elements of the drop. In this manner, the mesh of the interface and the algebraic system of equations of the boundary elements is smaller than those of other more conventional numerical schemes, such as e.g., finite differences.

3.2 Numerical Accuracy

The numerical simulation presented in this paper uses a surface of *2048* elements. To obtain the *time evolution* of the drop deformation, time is advanced using a fourth-order Adams-Bashforth-Moulton method [16]. The total time required to reach the stationary shape of the drop is $T = Gt$, reaching the final stationary deformation in all numerical experiments. These numerical results were compared with the data reported by Rosas [10] under the same flow regime.

4. Results

The numerical experiments explore effects of the applied flow on the drop shape. Figure 2 shows the evolution of the drop shape with the application of steady flow conditions. The drop evolves from the initial spherical shape to a final ellipsoidal form. The simulation is stopped when the drop deformation no longer changes; see figures 2 and 3. The deformation values attained numerically are those obtained experimentally from Rosas [10] within $\pm 5\%$ for $0.05 \le Ca \le 0.25$ and $\pm 1\%$ for $0.3 \le Ca \le 0.4$.

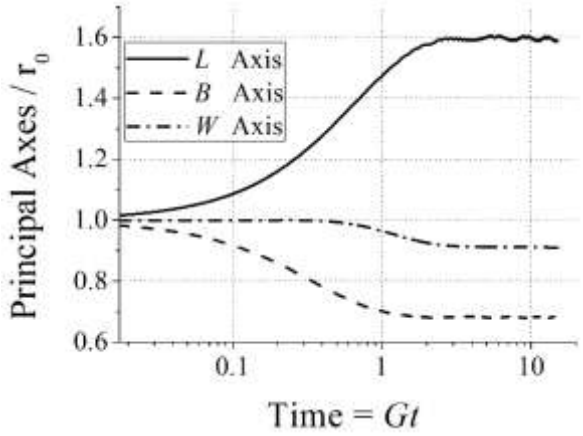

Figure 2. Evolution of the three principal axes of the drop in a flow with $\alpha = 0.13$, $Ca = 0.4$ and Total time $Gt = 15$.

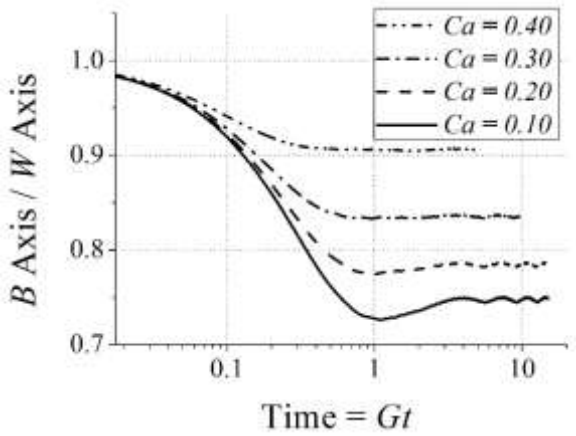

Figure 3. Ratio of the B wrt the W axes in numerical simulations for a flow with $\alpha = 0.13$, and Total time $Gt = 15$; 3 different values of Ca.

Figure 2 shows that the stationary state is reached as early as *10%* of the total simulation time; the drop remains in the stationary shape for the rest of the simulation. Although small oscillations in the stationary values persist, the amplitude of these oscillations is less than *±1.5%* of the average long-time value.

As well, data for the *W*-axis indicates that the cross section of the drop is not circular, for *B* values are significantly smaller. To observe the non-symmetric form of the drop, the ratio of *B* vs. *W* is presented in figure 3. On one hand, it can be observed that, with $Ca = 0.4$, in the initial *10%* of the evolutions *B*/*W* decreases and undershoots its stationary value. On the other hand, the rates of change for *B* and *L* are very similar, and are mainly determined by the magnitude of the vorticity. However, the increment of *W* wrt *B* clearly occurs at a faster pace; actually, based upon figure 3, the rate appears to be about four times faster for $Ca = 0.4$. The time evolution of the *B* and *W*-axis are different, as seen by the rate of change for the cross section axes, i.e., the *B*-axis changes at a rate similar to that of as the *L*-axis, while the rate of rotation of the *W*-axis begins to change immediately at the onset of the flow. However, the *W*-axis lags in time. Up to the time $Gt = 1$, the *W*-axis does not change. Then the *W*-axis changes about the time when the other two axes have reached their stationary value.

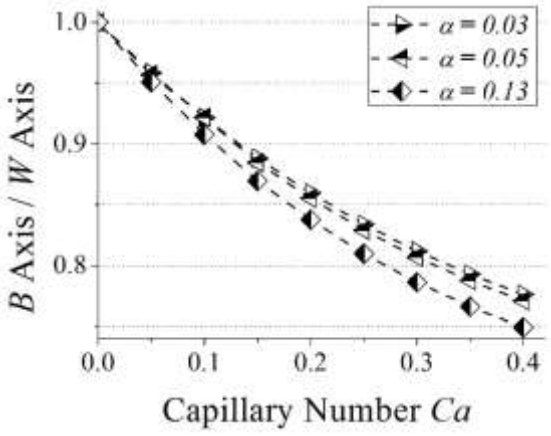

Figure 4. Stationary ratio of B wrt W axes in numerical simulations for a flow with $\alpha = 0.03$, $\alpha = 0.05$ and $\alpha = 0.13$ for different values of Ca.

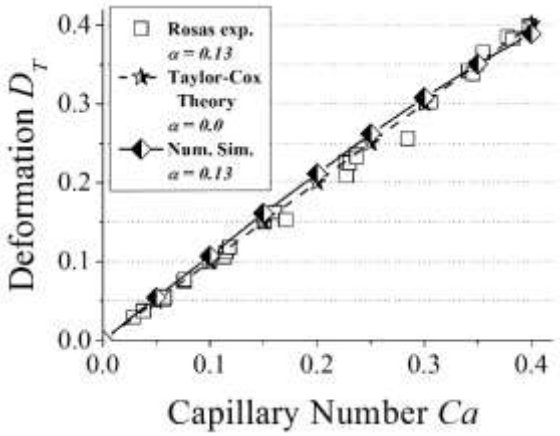

Figure 5. Stationary Taylor Deformation values for numerical simulations and experimental data for $\alpha = 0.13$ and analytical results of Taylor-Cox at $\alpha = 0.0$ for different values of Ca.

In figure 4 the ratio between axes of the cross section of the drop are given for three different flow strengths. As the capillary number increases, the eccentricity of the ellipsoid of the cross section increases as well. This ratio also depends on the flow-type parameter α becoming more eccentric for flows close to simple shear flow. For simple shear flows, these simulations produce values for the ratios of the cross section that are similar to the numerical results reported in References [7,8], having as well the same general behavior, even though the viscosity ratio reported is larger. Qualitatively it is possible to see the similarity [8]. Figure 5 presents a comparison of experimental results [10] and the simulated values for $\alpha = 0.13$, and the analytical results of Taylor-Cox for $\alpha = 0.0$ for the stationary Taylor Deformation value in the xy-plane; see figure 1(b).

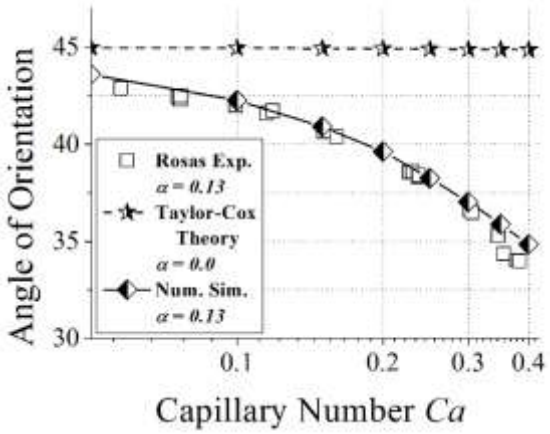

Figure 6. Orientation of the drop for numerical simulations and experimental data for $\alpha = 0.13$ and analytical results of Taylor-Cox $\alpha = 0.0$ for different values of Ca.

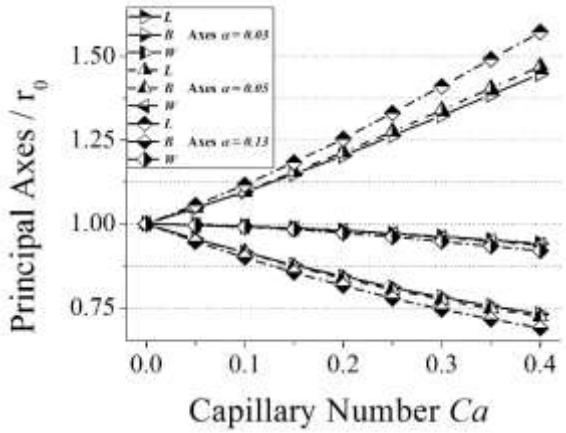

Figure 7. Stationary values of the principal axes of the drop for a flow with $\alpha = 0.03$, $\alpha = 0.05$ and $\alpha = 0.13$ for different values of Ca.

The stationary deformation of the drop depends upon the capillary number as well as the flow type. When $Ca = 0.4$, and for flows with $\alpha = 0.03$, the deformation achieved is less than *85%* of the values reached for flows of $\alpha = 0.13$. Cox [5] and Taylor [1] theory for simple shear flows establishes a linear relationship between deformation *vs*. the capillary number. However, the dependence observed with simulations of stronger flows is no longer linear, the later being in agreement with the experiments of Rosas [10, 11].

Figure 6 shows the rotation of the principal axis of the drop; see figure 1 (b). In figure 6, the orientation is comparable with the experimental data for similar capillary numbers. The theory based in

simple shear flow does not match with the experimental data. Finally, the measurements of the principal axes of the drop are shown in figure 7. These values were obtained in the stationary shape of the drop.

5. Conclusions

The simulations here presented for drop forms induced in 2D-flows do not appear to match the axisymmetric case established by G. I. Taylor and Cox, as neither did Kennedy et al., and Guido et al., for the simple shear flows. This is likely the case for capillary number less than *0.4*.

For $Ca > 0.4$, the deformation in the *xy*-plane increases, but, neither as numerical simulation show, there is a correlation with the Taylor-Cox model. On the other hand, the simulated behavior appears consistent with the experimental data of Rosas.

The difference between the simple shear flow, $\alpha = 0.0$, and flows with stronger degree of elongation induced larger drop deformations while the angle of orientation (principal axis) rotates away from *45* degrees.

The analysis of the *L*, *B* and *W*-axes of the ellipsoidal drop, in steady state, clearly show deviations from the axisymmetric shape as the flow type parameter α increases. However, the change of *W* remains unchanged for the values $\alpha = 0.03 - 0.13$, as a result of the vorticity of the applied 2D-flow.

6. Acknowledgments

The authors acknowledge funding provided by Project No. IG100714 of PAPIIT-UNAM Program. ASS gratefully acknowledges the financial support provided by CONACyT and PCeIM-UNAM during his PhD studies.

7. References

[1] Taylor G I 1932 *Proc. Roy. Soc.* A **138** 41
[2] Taylor G I 193. *Proc. Roy. Soc,* A **146** 501
[3] Rallison J M 1984 *Ann. Rev. Fluid Mech*. **16** 45
[4] Prosperetti A and Tryggvasson G 2009 *Computational Methods for Multiphase Flow* (Cambridge, New York, Melbourne: Cambridge University Press)
[5] Cox R G 1969 *J. Fluid Mech.* **37** 601
[6] Hinch E J and Acrivos A 1980 *J. Fluid Mech.* **98** 305
[7] Guido S and Villone M 1999 *J. Rheol.* **42**(2) 395
[8] Kennedy M R, Pozrikidis C and Skalak R 1994 *Computers Fluids*. **23**(2) 251
[9] Bentley B J and Leal L G 1986 *J. Fluid Mech.* **167** 241
[10] Rosas I Y, Reyes M A H, Minzoni A A and Geffroy E 2015 *Exp. Therm. Fluid Sci.* **60** 54
[11] Escalante C A, Reyes M A H, Rosas I Y and Geffroy E 2015 *J. Phys.: Conf. Ser*. **582** 012014
[12] Leal L G 2007 *Advanced Transport Phenomena* (Cambridge, New York: Cambridge University Press)
[13] Pozrikidis C 1997 *Introduction to Theoretical and Computational Fluid dynamics* (New York, Oxford: Oxford University Press)
[14] Reyes M A H, Minzoni A A and Geffroy E 2011 *J. Eng. Math*. **71**(2) 185
[15] Macosko C W 1994 *Rheology Principles, Measurements, and Applications* ed Wiley-VCH (Chichester New York) p21-23 68-74
[16] Lambert J D 1973 *Computational Methods in Ordinary Differential Equations* ed Wiley & Sons (Chichester New York)